# The influence of aggregate texture, morphology and grading on the carbonation of non-hydraulic (aerial) lime-based mortars

**A. Arizzi*** **& G. Cultrone**

Universidad de Granada, Departamento de Mineralogía y Petrología, Campus Fuentenueva s/n, 18002 Granada, Spain

*Corresponding author (e-mail: arizzina@ugr.es)

**Abstract:** This paper reports on investigations of the influence of the texture, morphology and grading of fine aggregates on the microstructure and macroscopic properties of aerial lime-based mortars. To understand the role of the aggregate in the outcome of the carbonation process, mortars set with two aggregates were cured for 2 years under standard conditions and studied at different time intervals by means of textural and mineralogical analyses and hygric and physical–mechanical tests. Both the initial and further development of the mortar properties are strongly influenced by compositional and textural differences induced by the type of aggregate used. Results show that a calcareous aggregate with continuous grading, consisting of sub-angular grains with a rough surface, induced better textural and physical–mechanical properties than a siliceous aggregate, with polished surface grains and less continuous grading. The use of a calcareous aggregate also provided compositional continuity between the binder and aggregate, apparently promoting further improvement in carbonation and physical–mechanical properties. Further work to quantify this influence is recommended.

Lime-based mortar has been widely used as a structural and ornamental material for at least the past 10000 years, until the 19th century. A significant portion of the worldwide architectural heritage is constructed with brick or stone blocks bound together with this type of mortar, especially in Europe, America, North Africa and West Asia. The most ancient archaeological examples of lime and gypsum mortars have been found in the cities of Yftah (Israel) and Çatalhöyük (Turkey) (7000–6000BC) and in the Egyptian pyramids (4000–2000BC). In Europe, the greatest examples of the ample range of construction ability achieved with mortars date back to Greek and Roman times. Furthermore, mortars are often applied as finishing or decoration layers to provide a protective, smooth and attractive finish (Groot 2010; Veiga 2010). As examples of ornamental mortars, it is worth mentioning the stuccos of the Mayan and Inca civilizations (AD300–900), and the gypsum plasters of the Alhambra Moorish palaces of Granada (14th century, Spain).

Mortars are basically composed of aggregates and a binder, and the latter is the defining component of a mortar. Lime has been the preferred binder used in monuments and historical buildings. Two main types of lime, aerial (also called non-hydraulic lime) and hydraulic, are distinguished according to the initial composition of the carbonatic stone (i.e. limestone, dolostone and marble) used and the hardening reactions occurring during mortar setting. Aerial lime is obtained from a fairly pure carbonatic stone, which is burnt at 600–800 °C to obtain a highly reactive calcium oxide (quicklime, CaO) that turns into calcium hydroxide (slaked lime or portlandite, $Ca(OH)_2$) after hydration. Aerial lime hardens when exposed to air, as it reacts with the atmospheric $CO_2$, transforming into $CaCO_3$, according to the following reaction:

$$Ca(OH)_2 + CO_2 \rightarrow CaCO_3 + H_2O. \quad (1)$$

If the original stone also contains magnesium carbonate, the resulting lime will be a dolomitic or magnesian lime that is composed of brucite ($Mg(OH)_2$) in addition to portlandite.

Hydraulic lime is obtained by burning, at a temperature of about 1000 °C, a carbonatic stone containing silica and alumina impurities or a mixture of the stone with a clay. On addition of mixing water, the initial hardening process of this lime occurs through the relatively rapid reaction of Si and Al with portlandite to produce strength-promoting calcium silicate and aluminate hydrates. For this reason, hydraulic lime is able to set under water; however, as portlandite comprises a high proportion of the binder, continuing carbonation in air remains an important reaction for long-term strength and durability.

In the case of mortars in which aerial lime is the binder, hardening occurs only as a result of the carbonation process, during which portlandite is transformed into the less soluble calcite, thus causing an increase in weight and in volume of 35% and 11.8%, respectively.

The reaction presented above involves three main stages: (1) diffusion of $CO_2$ within the material; (2) dissolution of $CO_2$ and $Ca(OH)_2$ in the pore water; (3) precipitation of $CaCO_3$. Key influences on these stages include $CO_2$ permeability, relative humidity and temperature (Moorehead 1986; Houst & Wittmann 1994; Sánchez-Moral *et al.* 2004; Van Balen 2005). It is important to note that relative humidity and $CO_2$ concentration are crucial factors in the mineralogy (polymorphs formed), morphology and size of the calcium carbonate crystals formed at different stages of the carbonation process (Cizer *et al.* 2012; Gomez-Villalba *et al.* 2012).

In general, the carbonation process causes an increase in density and strength, and a change in the pore system of the mortar (Ngala & Page 1997; Lawrence *et al.* 2007). However, in most cases, these changes take a long time, because the formation of calcite at the expense of portlandite decreases the porosity and reduces the

*Quarterly Journal of Engineering Geology and Hydrogeology,* Vol. **46**, 2013, pp. 507–520
doi: 10.1144/qjegh2012-017
Published *Online First* on October 31, 2013

permeability of the material to $CO_2$, thus slowing the process down. The diffusion of $CO_2$, governed by Fick's and Knudsen's laws, depends strongly on the pore size and geometry of the mortar (Houst & Wittmann 1994), and is generally higher (and the carbonation enhanced) at the interface between the surface of the grains and the matrix (ITZ, interfacial transition zone) than in the matrix itself (Bourdette *et al.* 1995). An increase in porosity in this area was observed by Lawrence *et al.* (2007), who attributed it to the formation of amorphous and semi-amorphous calcium carbonate aggregates at the border of the grains.

The characteristics of the lime particles (shape, size and aggregation) influence the speed of carbonation and the performance of the final product (Cazalla *et al.* 2000; Rodriguez-Navarro *et al.* 2002, 2005; Ruiz Agudo & Rodriguez-Navarro 2010).

Moreover, the presence of non-carbonated areas in an apparently carbonated mortar is due to the heat released (74 kJ $mol^{-1}$) during the carbonation reaction, which is sufficient to evaporate the water produced by the reaction and sometimes also the free and capillary water in the paste (Moorehead 1986).

Finally, the environmental conditions in which lime-based mortars are cured (especially moisture produced by wetting–drying cycles) influence their final mechanical performances and durability (El-Turki *et al.* 2010).

It is evident that all the factors that affect the microstructure of the mortar influence the outcome of this process. For this reason, during the preparation of mortars the components and their proportions must be selected carefully to ensure the best textural properties. In a non-carbonated mortar, the total porosity and the pore size distribution (PSD) depend to a large extent on the binder-to-aggregate (B/A) and water-to-binder (W/B) ratios, the binder composition, the presence of additives and also the shape and grading of the aggregate (Lanas & Alvarez-Galindo 2003). In general, aggregates with an angular shape, rough surface (crushed aggregates) and large surface area need more water than round aggregates with a smoother surface (natural aggregates; Westerholm *et al.* 2008). In addition, aggregates with continuous grading produce a well-packed system in which voids between grains of the same size are filled by smaller grains, thus reducing the porosity (Romagnoli & Rivasi 2007; Fung *et al.* 2008; Kwan & Fung 2009). Water content varies depending on the properties of the fine aggregate (equivalent particle size <4 mm; Westerholm *et al.* 2008), that is, the particle shape, surface area, porosity, roughness and roundness. The best aggregate is described as a well-graded sharp sand (i.e. medium to coarse sand; NHBC Foundation 2008) with a partially angular shape; the reason is that this type of aggregate generates a good interlocking, void filling and surface adhesion. The worst aggregate is a single-size rounded sand with a polished surface; this type of aggregate interlocks poorly and the binder also adheres poorly to it.

Previous research has shown that the use of different aggregates produces mortars with different microstructures (Venkatarama & Gupta 2007). Moreover, as the carbonation process is strongly influenced by the microstructure, the velocity of transformation of portlandite into calcium carbonate is likely to vary depending on the aggregate used. Furthermore, aggregates with the right shape and grading improve the textural and mechanical properties of the mortar. Finally, aggregate mineralogy is another factor to consider, especially with regard to mortar durability. Siliceous aggregates composed exclusively of quartz are abundant in much of the world and provide a chemical resistance to the attack of sulphates and others salts; this is why these aggregates are so commonly used in mortars. By contrast, a calcareous aggregate is weaker than quartz and more easily damaged by salt crystallization and contamination agents, especially if dolomite is present.

The indirect role of aggregate in the carbonation process, then, is evident because (1) the shape and grading of the aggregate influence the microstructure of the mortar paste (i.e. the pore system), whereas its mineralogical composition mostly influences the mechanical properties and the durability of the hardened mortar; (2) the speed and the degree of carbonation depend on the pore characteristics of the paste; and (3) the formation of calcite leads to changes in the pore system of the mortar.

The objective of this work is to follow the microstructural and macroscopic modifications caused by the carbonation process in mortars made with two natural aggregates. The two aggregates selected have different grading, mineralogy (calcite and quartz) and morphology (grain shape and texture). Moreover, they were produced by different processes: extraction and crushing in the case of the calcareous aggregate; excavation and washing in the case of the siliceous aggregate. These two aggregates, with opposite characteristics, were selected because they are two of the most common aggregates produced and marketed in the Andalusian region (southern Spain). Although a huge variety of aggregates is nowadays available, often economic constraints oblige builders to use one specific type of aggregate, which is easily available from the nearest outcrop but which could be inappropriate. In view of the specific constraints of one geographical area and taking into account the characteristics, discussed above, required for an aggregate, this work aims to present and study in detail two extreme scenarios that are likely to arise during the making of mortars.

# Materials and methods

## Components of mortars

### Binder

The binder used in the preparation of the mortars is a dry hydrated lime (CL90-S, AENOR 2002) supplied by ANCASA (Seville, Spain).

### Aggregates

Two aggregates from southern Spain (Andalusian area) were used for mortar preparation: a granular siliceous aggregate (SA) from Arcos de la Frontera (Cadiz, Spain), marketed by Sibelco Minerales, and a crushed calcareous aggregate (CA), produced in the Darro plant (Granada, Spain). According to the European standard classification for aggregate grading (AENOR 1996), both SA and CA can be classified as fine aggregates; their grading is shown in Table 1.

### Characterization of binder and aggregates

The chemical composition (major and minor elements) of the components of mortars was studied by X-ray fluorescence spectrometry (XRF) using a Bruker S4 Pioneer system, with wavelength dispersion equipped with a goniometer that analyses crystals (LIF200/PET/OVO-55) and a Rh X-ray tube (60 kV, 150 mA). Semi-quantitative scanning spectra were obtained using Spectraplus software. Sample powders (*c.* 5 g) were dispersed in KBr, deposited in an aluminium cup and then pressed at 10000 kg to obtain a pressed pellet (40 mm diameter sample disc). Measurements were performed in a vacuum with a rotating sample.

The mineralogical phases of binder and aggregates were determined by X-ray diffraction (XRD) and thermogravimetric analysis (TGA). In the first case, we used a Panalytical X'Pert PRO MPD, with automatic loader. Analysis conditions were as follows: CuKα radiation (λ = 1.5405 Å), 4–70 °2θ explored area, 45 kV voltage, 40 mA current intensity, and goniometer speed 0.01 °2θ $s^{-1}$ using a Si-detector X'Celerator. The interpretation and quantification of the mineral phases was performed using the X-Powder software

**Table 1.** *Cumulative percentage of calcareous (CA) and siliceous (SA) aggregate grains passing each sieve size*

| Sieve size (mm) | Cumulative percentage | |
|---|---|---|
| | CA | SA |
| 1.6 | 100.0 | 100.0 |
| 1.0 | 78.0 | 99.8 |
| 0.8 | 65.9 | 99.7 |
| 0.5 | 57.1 | 99.4 |
| 0.25 | 44.9 | 52.2 |
| 0.125 | 25.5 | 0.9 |
| 0.063 | 18.0 | 0.9 |
| <0.063 | 0.0 | 0.0 |

package (Martín Ramos 2004). Thermal measurements were made with a Shimadzu TGA-50H analyzer. Approximately 50 mg of sample was heated in an aluminium crucible, in a flushed-air atmosphere (100 ml $min^{-1}$), at a heating rate of 5° $min^{-1}$ over a range of 25–950 °C. TGA data treatment was carried out according to the AENOR standard (AENOR 1997).

## Mortar preparation

Two types of mortar were prepared with a binder to aggregate ratio of 1:3 by weight. Owing to density differences between the two aggregates used, with regard to volume ratio this approximates to a 1:1 ratio for the CC mortar (CL + CA) and a 1:1.2 ratio for the CS mortar (CL + SA). A recommended dosage exists for every type of mortar, depending on its function in the building (e.g. structural, rendering, grouting mortars, etc.). In this case, we aimed at a volume ratio close to 1:1 as this is the most common ratio for rendering mortar (mortar applied to cover an exterior surface; Azconegui *et al.* 1998). The dosage has been expressed by weight (1:3) to simplify the mixing of dry components during the mortar preparation. The use of weight to determine the B/A ratio would cause the CC samples to receive a proportionately greater amount of binder; however, this difference is considered to be relatively minor in the context of the overall results. The preparation and curing of mortar samples were carried out following accepted standards (AENOR 1999*a*, 2000), with the modifications proposed by Cazalla (2002), regarding the curing conditions and time: mortars were cured at $T = 20 \pm 5$ °C and relative humidity (RH) = 60 ± 5%, instead of at an RH of 95%, and they were removed from the moulds after 7 days, instead of after only 3 days.

After carefully weighing and mixing the binder and the aggregate in the dry state, these were poured into a stainless steel container in which the water required for mixing had been previously added. The amount of water for each mixture was established according to the flow test (AENOR 1999*b*), to obtain mortars with a plastic consistency. The flow, calculated as the average of the spread diameter (in mm) measured on three fresh samples, was in the range of 150–200 mm. The mortar mixing was carried out in an automatic mixer that ensured a uniform distribution of all the component particles within the fresh mortar mixture. Mixing was carried out for 90 s at slow velocity, as indicated in the AENOR (1999*a*) standard.

Normalized stainless steel moulds (AENOR 1999*a*) with three separate sections of 4 cm × 4 cm × 16 cm each were used for the casting of the mortars. The internal surfaces of the moulds were lightly lubricated with a very low-viscosity non-resin mineral oil to avoid excessive adhesion of the fresh mortar to the surfaces and thus ease the subsequent removal from the mould (AENOR 1999*a*). The moulding was carried out by pouring the fresh mixture into the mould, filling the lower half, and then compacting the mortar by striking it 15 times with a metal bar. Following this, the upper half of the mould was filled and the mortar was struck 15 more times to compact it in the mould (AENOR 1999*a*). Excess material was removed with a ruler inclined at 45° that left the surface flat and without depressions.

Mortars were cured under controlled conditions of temperature (20 ± 5 ºC) and RH (60 ± 5%) for 7 days, as proposed by Cazalla (2002), instead of being cured at an RH of 95% for 5 days, so as to ensure a sufficient hardening of the mortars. After removal from the moulds, mortars were cured at the same laboratory conditions throughout the study. In total, 70 samples were prepared for each mortar type.

## Mortar characterization

To monitor the mineralogical, textural and physical changes in the mortars owing to the carbonation process, the mortar samples were analysed after 7, 15 and 28 days, 2 and 6 months and 1 and 2 years.

### Study of the carbonation degree of the mortars

The mineralogical phases of the mortars were determined by XRD and TGA using the same analytical devices as described above. In the latter technique, mortar phases and their amounts were determined by measuring the weight loss resulting from the stoichiometric reactions of portlandite dehydroxylation (450< $T$ <550 °C) and calcite thermal decomposition (700< $T$ <900 °C). The decrease in portlandite content was taken as a reference to estimate the carbonation degree index ($I_{CD}$, in %) at the same time intervals as indicated above, according to the equation (Arizzi *et al.* 2012)

$$I_{CD} = \frac{CH_0 - CH_x}{CH_0} \times 100 \quad (2)$$

where $CH_x$ is the amount of portlandite at time $x$ and $CH_0$ is the initial content of portlandite (at time zero). In this calculation, the decrease in the amount of portlandite can be related to only the carbonation process, whereas the variations in the amount of calcite depend also on the presence of the calcareous aggregate. For this reason, it has been preferred to consider the decrease in the portlandite content instead of the increase of the calcite content to better study the evolution of the carbonation process.

Both inner (core) and outer (1 $cm^3$ from the surface to the core) parts of the mortar samples were analysed periodically. Samples for XRD and TGA were prepared by grinding homogeneously a representative piece of the mortar (of around 2 $cm^3$) until it was reduced to a powder. This method ensures that both the binder and the aggregate portions are mixed in the sample; therefore the mineralogical composition obtained is representative of the whole mortar.

### Textural characterization of the mortars

The inner and outer areas of the microstructure of the mortars (morphology, cohesion, porosity) were observed using optical microscopy (OM) and field emission scanning electron microscopy (FESEM). In the first case, thin sections were observed using an Olympus BX-60 microscope equipped with a digital microphotography camera (Olympus DP10). In the second case, a Carl Zeiss Leo-Gemini 1530 microscope was used to analyse previously dried, carbon-coated mortar fragments. FESEM was also useful for observing aggregate morphology at a micro-scale

whereas the use of OM on hardening mortars allowed assessment of the cohesion in the area between the aggregate grains and the matrix.

### Pore system of the mortars

The pore system was evaluated using two complementary techniques: mercury intrusion porosimetry (MIP) and $N_2$ adsorption. Open porosity ($P_o$, %) and pore size distribution (PSD, in a range of $0.002 < r < 200\,\mu m$) were determined using a Micromeritics Autopore III 9410 porosimeter. Mortar fragments of *c.* 1 $cm^3$ collected in the internal and external areas were oven-dried for 8 h at 100 °C before analysis. A Micromeritics 3000 Tristar system was used to obtain $N_2$ sorption isotherms ($T = 77$ K) under continuous adsorption. Before the measurements, samples were heated to 110 °C for 4 h and outgassed to $10^{-3}$ Torr using a Micromeritics Flowprep. Specific surface area (SSA) was determined according to the BET method (Barret *et al.* 1951) by means of $N_2$ adsorption measurements, because this technique is more precise than MIP especially in the range of smallest pores (when 'ink-bottle' pores are analysed, the smallest pores are overestimated and the largest ones are underestimated). The BJH method (Brunauer *et al.* 1938) was applied to determine PSD and pore volume (in a range of $15 < d < 500$ Å).

### Hygric properties

Free water absorption, drying and capillary uptake tests were performed to study the hygric properties of the mortars. Hygric tests were not performed until the mortars had been cured for 28 days, because 'younger' mortars are less compact and therefore lime may dissolve in water. Mortar samples were oven-dried at 100 °C for 24 h before measurements were taken. The absorption and drying kinetics were evaluated on three samples (4 cm × 4 cm × 4 cm) per type by measuring the changes in the mass of mortar samples over time owing to water flux within the pore system. The absorption coefficient ($C_a$) was determined as the slope of the first two points in the curve representing the weight increase as a function of the square of time (4 min after the beginning of the test) (UNI-EN 13755, CNR ICR 2008). The drying index ($I_d$) was measured according to the NORMAL 29-88 standard (CNR-ICR 1988). The capillary uptake was performed on three samples of 4 cm × 4 cm × 16 cm. Two imbibition coefficients ($A$ and $B$) were determined from the mass uptake per surface unit and the height over time, according to the Beck *et al.* (2003) procedure.

### Physical–mechanical properties

Flexural and compressive strengths were measured by means of an INCOTECNIC-Matest hydraulic press. According to the EN 1015-11 standard (AENOR 2000), flexural tests were carried out on three samples per mortar (of 4 cm × 4 cm × 16 cm). The six samples obtained after the flexural rupture were used for the compressive tests.

The ultrasonic wave propagation technique was also used to determine the elastic–dynamic properties of mortars, which are related to their mechanical resistance and density. Measurements were performed using a Panametrics HV Pulser/Receiver 5058 PR coupled with a Tektronix TDS 3012B oscilloscope, in transmission–reception mode. A couple of non-polarized piezoelectric transducers were used, with a frequency spectrum of 1 MHz. Measurements were carried out on three mortar samples per type, of 4 cm × 4 cm × 16 cm, along three perpendicular directions: *a*, parallel to the compaction plane; *b*, parallel to the compaction plane along the largest face of the sample; *c*, perpendicular to the compaction plane. The velocity of propagation of primary ($V_p$) and secondary ($V_s$) waves within the mortar samples was determined as the ratio between the specimen length and the transit time of the pulse.

Once the average values of $V_p$ and $V_s$ were determined along *a, b* and *c* directions for three samples of each type of mortar, and knowing the bulk density ($\rho_b$, g $cm^{-3}$) of the mortar for each case, the Poisson ratio ($\nu$) and the stiffness ($G$), Young's ($E$) and compressive ($K$) moduli of the mortars were calculated using the following equations:

$$\nu = \left[\left(\frac{V_p}{V_s}\right)^2 - 2\right] \Big/ \left[2\left(\frac{V_p}{V_s}\right)^2 - 1\right] \quad (3)$$

$$G = \rho_b V_s^2 \quad (4)$$

$$E = 2G(1+\nu) \quad (5)$$

$$K = \frac{E}{3(1-2\nu)}. \quad (6)$$

# Results and discussion

## Characteristics of the aggregates

By means of FESEM, the morphological and textural characteristics of the finest fraction of the two aggregates were observed. Figure 1a shows that the calcareous grains (CA) have irregular edges and their surface is composed of micrometre-sized crystals of calcite that make the aggregate rough and porous (Fig. 1c). The siliceous grains (SA), instead, are more rounded and their surface is smoother and presents few discontinuities (Fig. 1b and d).

Using optical microscopy, it was possible to observe the textural differences existing between the biggest grains of the two aggregates. The calcareous grains (Fig. 2a and b) are sub-angular and heterogeneous in shape, especially those grains with a diameter greater than 0.5 mm in size that appear more ellipsoidal than spherical. The siliceous grains (Fig. 2c and d) have a more homogeneous shape compared with the calcareous ones.

The morphological characteristics of the two aggregates depend on their nature and the production processes involved. The calcareous aggregate proceeds from a rock outcrop and its production involved extraction and crushing processes that made the grains angular and rough, whereas the siliceous aggregate was obtained by excavation and subsequent washing, processes that did not alter the surface of the quartz grains, which remained smooth and sub-rounded.

Table 2 shows the chemical and mineralogical composition of the lime and aggregates used, characterized by the absence of impurities.

## Water dosage of the mortars

Different water dosages were used to obtain mortars with a similar consistency (see the section on mortar preparation). Generally, under the same composition and proportion conditions, differences in the amount of kneading water depend on the absorptiveness of the aggregate, which is in turn related to its particle shape (Gonçalves *et al.* 2007) and fineness. The values of specific surface area of the two aggregates, determined by $N_2$ adsorption, explain why more water is required in the preparation of CC mortars (31%) than CS (27%); the SSA was found to be much

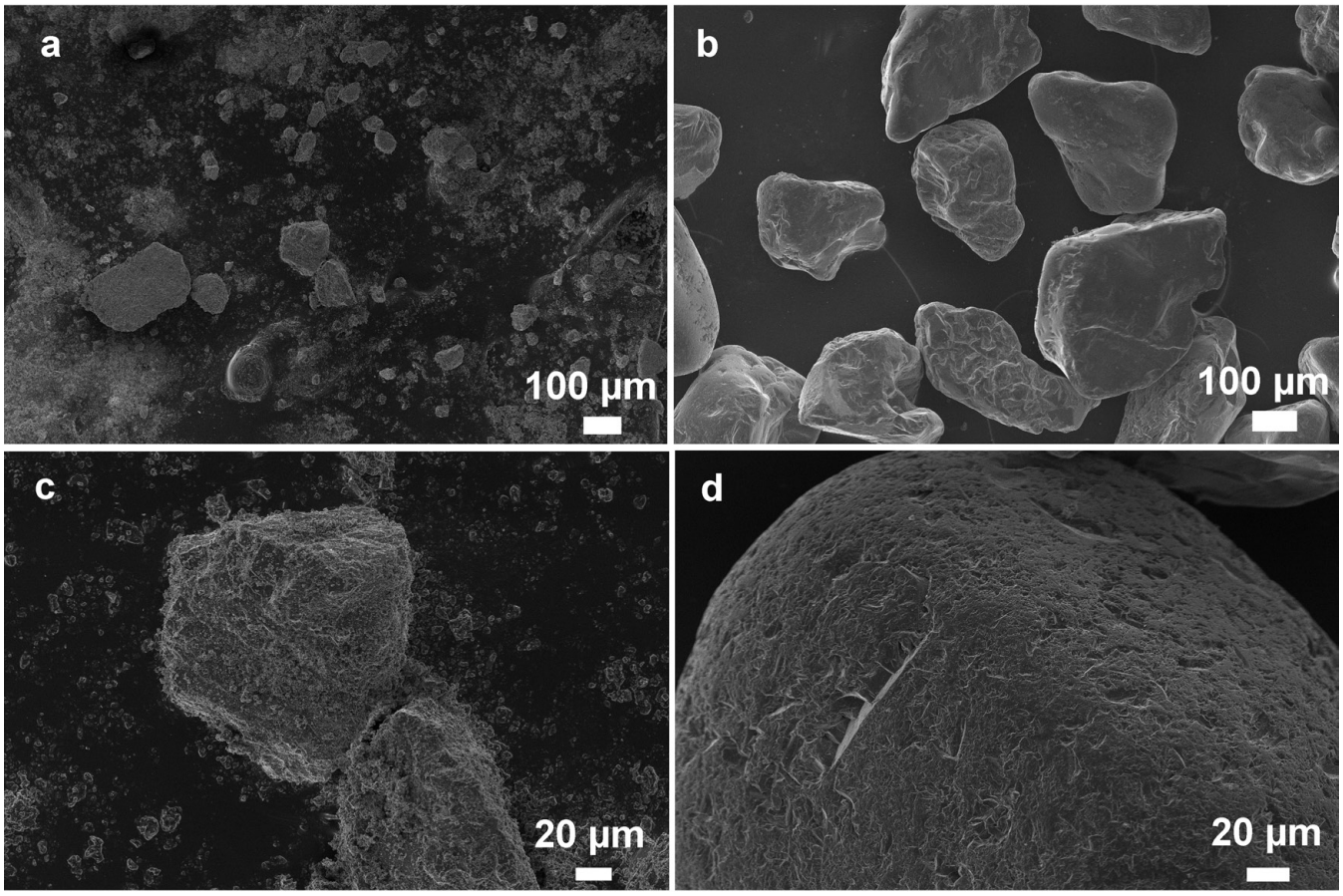


**Fig. 1.** FESEM images showing the texture of the smallest fraction of the calcareous (**a**, **c**) and siliceous (**b**, **d**) aggregates at different magnifications.

higher in CA ($0.6555\,m^2\,g^{-1}$) than in SA ($0.0493\,m^2\,g^{-1}$). The higher SSA value found for CA is explained by the higher fineness of this aggregate (Table 2), the presence of rock dust (micrometre-sized crystals observed in Fig. 1a and c) on the surface of the CA grains, and the oblate and angular shape of these grains. These characteristics of the calcareous aggregate, which are the result of both the crushing process and the medium hardness of the calcite mineral, are responsible for the larger amount of water used for the preparation of CC mortars.

## Carbonation degree of the mortars

The quantification of the mineral phases was carried out from the initial amounts of calcite, portlandite and quartz in mortars determined by XRD and TGA. Knowing that 96% of the lime (CL) is portlandite (Table 2) and that the binder represents 25% of the total mass, the initial amount of portlandite was calculated as 24%. Both XRD and TGA techniques show that portlandite content decreases over time, a process that occurs more quickly on the exterior of the mortars than on the inside, because carbonation progresses from the surface to the core (Cazalla 2002; Lawrence *et al.* 2006).

The fall in the portlandite content of the mortars over time is an indicator of the carbonation degree, which is expressed here as $I_{CD}$ (in %). This parameter was calculated according to equation (2) and is represented as a function of time in Figure 3. As has been observed in other studies on similar materials (Arizzi *et al.* 2013), carbonation of the outer part of mortars occurs very quickly within the first 2 months of curing (at 28 days for CS and at 2 months for CC), when the carbonation degree reaches almost 75% in both types of mortar. From this point onwards the $I_{CD}$ increases much more slowly (about 1% per month), and after 2 years reaches 89% in the outer part of CC as compared with 80% for CS. The carbonation reaction is enhanced in the CC mortar owing to both the compositional continuity of the mortar system (Cazalla 2002) and the grain morphology. In fact, calcite precipitates more readily in the nucleation sites of aggregates whose grains have an angular shape and a rough surface, such as calcareous aggregates (Lanas & Alvarez-Galindo 2003). The curve for the surface of the mortars shows a slight final slope that suggests that carbonation is still continuing in this area after 2 years of curing.

The trend of the curves showing the carbonation of internal samples indicates that carbonation is much lower inside the mortar than on the surface, owing to the fact that it is difficult for $CO_2$ to diffuse from a carbonated network (i.e. the surface), which is less porous, to the non-carbonated part (i.e. the core) of the mortar (Houst & Wittmann 1994). Moreover, carbonation is much faster in CC internal samples during the first months of curing. This indicates that the CC mortar has a more open, more permeable pore network than the CS at the beginning of the process, as the values for open porosity also show (Table 3). After 2 years of carbonation, the degree of carbonation inside the mortars is 77% in CC mortars and 74% in CS mortars.

## Textural characteristics of the mortars

Carbonation led to an improvement in the cohesion of mortars, as indicated by the fall in the value of open porosity measured by MIP analyses and the reduction of pores and fissures observed by FESEM over 2 years (Fig. 4). Interestingly, CC

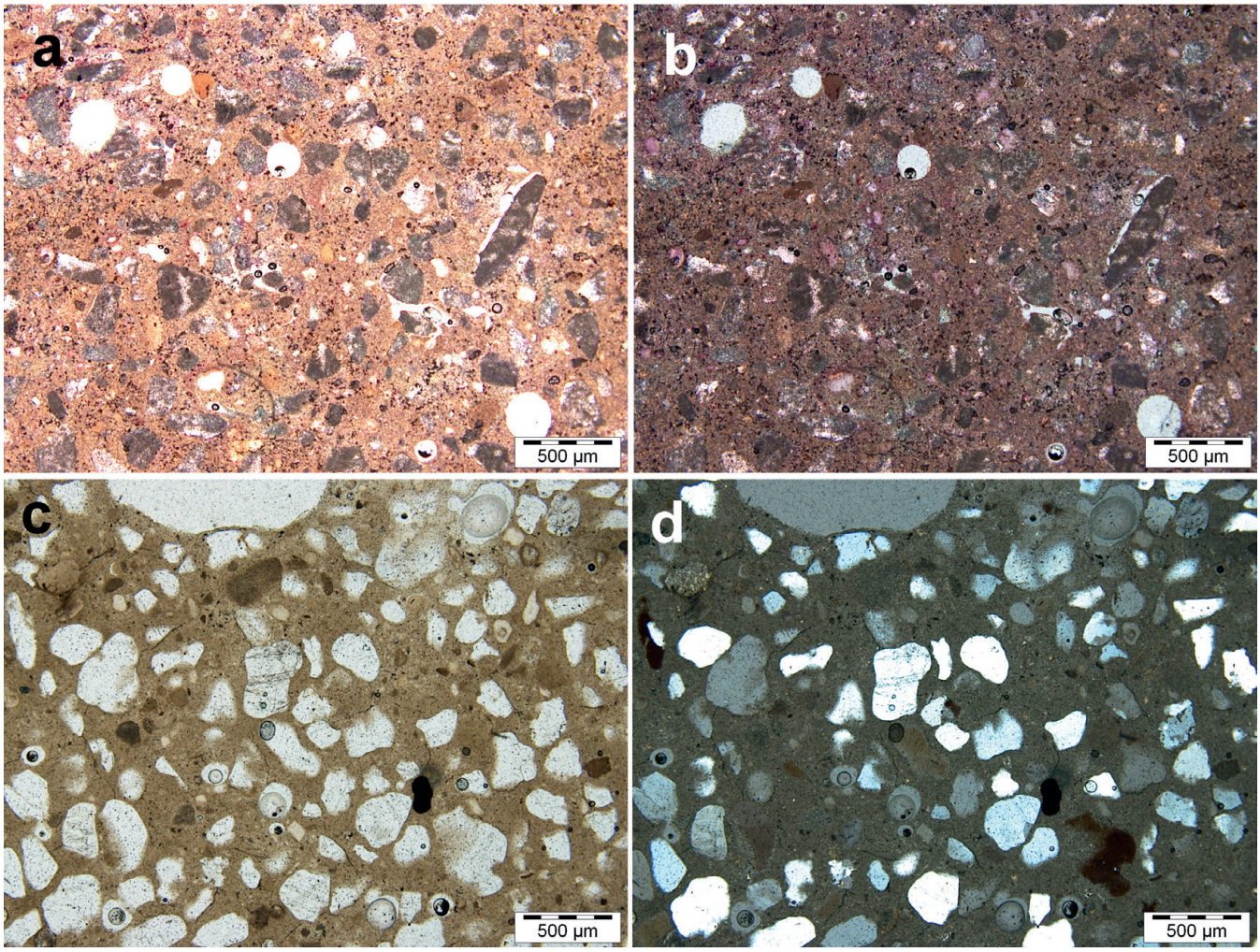


**Fig. 2.** OM images with plane (**a**, **c**) and crossed (**b**, **d**) polars of CC (lime mortar with calcareous aggregate) (**a**, **b**) and CS (lime mortar with siliceous aggregate) (**c**, **d**) mortars.

**Table 2.** *Chemical (XRF) and mineralogical (XRD) composition of calcitic lime (CL), calcareous (CA) and siliceous (SA) aggregates*

| | CL | CA | SA |
|---|---|---|---|
| *Chemical composition (XRF) (wt %)* | | | |
| $SiO_2$ | 0.35 | 0.16 | 95.11 |
| CaO | 78.01 | 59.59 | 0.35 |
| $SO_3$ | 1.39 | 0.03 | 0.05 |
| MgO | 0.70 | 0.87 | 0.25 |
| $Fe_2O_3$ | 0.10 | 0.04 | 0.21 |
| $Al_2O_3$ | 0.18 | 0.06 | 0.55 |
| $K_2O$ | 0.05 | 0.01 | 0.26 |
| $P_2O_5$ | 0.04 | 0.01 | 0.10 |
| *Mineralogical composition (XRD) (%)* | | | |
| CC | 3.8 | 100 | – |
| CH | 96.2 | – | – |
| Qtz | – | – | 100 |
| *Mineralogical composition (TGA) (%)* | | | |
| CC | 8.9 | 99.5 | * |
| CH | 87.1 | – | * |
| Qtz | – | – | * |

CC, calcite; CH, portlandite; Qtz, quartz.
*Thermogravimetric analysis (TGA) was not performed on SA because quartz undergoes only structural transformation (α quartz → β quartz) within the established temperature, with no weight loss.

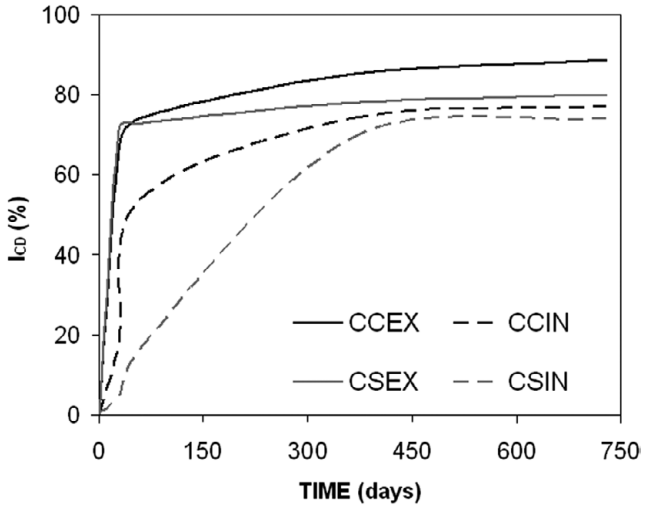


**Fig. 3.** Evolution of the carbonation process: carbonation degree index ($I_{CD}$, in %) represented as a function of the time (in days) for the outer (-EX) and inner (-IN) areas of CC (lime mortar with calcareous aggregate) and CS (lime mortar with siliceous aggregate) mortars after 28 days (28D), 2 months (2M), 6 months (6M), 1 year (1Y) and 2 years (2Y). $I_{CD}$ was calculated from the amount of portlandite obtained at each time interval by means of thermogravimetric analysis.

mortars, which were characterized by the worst textural properties over the first month (especially in the first week of curing, when the calcareous aggregate mortars had high porosity in the ITZ; Fig. 2a and b), showed a larger increase in density after the first year (Fig. 4a and c) and an improved cohesion between the matrix and the grain surface. The higher degree of carbonation recorded in CC mortars compared with CS at this time is responsible for this improvement. In contrast, it was observed that poor cohesion between the newly formed calcite and the surface of the siliceous grains in CS mortars existed even after 2 years of carbonation. In CS mortars some quartz grains are visible at different magnification (Fig. 4f), whereas in CC mortars it was almost impossible to recognize the calcareous grains, as their surface was completely covered by the newly formed calcite (Fig. 4e). However, it is possible that the visible quartz grains observed in Figure 4f are a result of the preparation of the sample before the FESEM observation.

## Pore system of the mortars

CC and CS mortars are mainly composed of pores with a radius of between 0.1 and 1 μm (Fig. 5), which is a structural peak typical of lime pastes, whose height depends on the amount of water initially added when mixing the mortars and that subsequently evaporated (Arandigoyen *et al.* 2005; Lawrence *et al.* 2007).

The porosity of CC mortars decreases during the first month (Table 3), the period in which the carbonation process is faster (Fig. 3), leading to a 12% increase in volume caused by the transformation of portlandite into calcite. The clearest result of the carbonation process in mortars is the rapid disappearance of the family of largest pores ($r > 1$ μm; Fig. 5b), which are filled by both microcrystalline and amorphous calcite (Moorehead 1986). This is because a mineral phase (calcite in this case) is more likely to precipitate inside the larger pores, where the energy required for their growth is lower than in the smaller pores (Rodriguez-Navarro & Doehne 1999). Interestingly, an increase in the porosity percentage is recorded from 1 to 6 months after the experiment began (Table 3) and this is due to an increase in the volume of pores in the 0.01–0.15 μm size range (Fig. 5a and b) This phenomenon was also observed by Lawrence *et al.* (2007) and is due to the formation of agglomerates of small calcite particles at the interface between aggregate grains and matrix. On the other hand, Arandigoyen *et al.* (2006) found that in lime and blended pastes the volume of pores with a radius of between 0.01 and 0.03 μm falls sharply during carbonation. This apparent discrepancy demonstrates the important influence of the aggregate on the microstructure of the mortar.

The volume of the smaller pores continues to increase until the end of the study, which confirms that carbonation is still continuing after 2 years.

No clear relation was found between carbonation time and the small variations of the size of the main family of pores ($0.1 < r < 1$ μm; Fig. 5b). During the first month, when most of the microstructural changes caused by the carbonation process took place, the main peak on the *x*-axis shifted slightly towards greater

**Table 3.** *Open porosity ($P_o$) and bulk density ($\rho_b$) obtained by mercury injection porosimetry (MIP), specific surface area (SSA) and pore volume obtained by $N_2$ adsorption, of lime mortars made with calcitic (CC) and siliceous aggregates (CS) at different time intervals*

| Time | $P_o$ (%) | $\rho_b$ (g cm$^{-3}$) | SSA (m$^2$ g$^{-1}$) | Pore volume (cm$^3$ g$^{-1}$) |
|---|---|---|---|---|
| *CC mortar* | | | | |
| 7D | 39.9(1.30) | 1.57(0.04) | 4.04(1.46) | 0.011(0.98 × 10$^{-3}$) |
| 15D | 35.2(1.68) | 1.55(0.04) | 4.13(0.79) | 0.013(2.25 × 10$^{-3}$) |
| 28D | 32.5(2.74) | 1.60(0.05) | 3.56(1.80) | 0.023(13.27 × 10$^{-3}$) |
| 2M | 35.0(1.10) | 1.65(0.04) | 3.35(0.74) | 0.021(4.80 × 10$^{-3}$) |
| 6M | 41.0(2.06) | 1.61(0.08) | 3.27(0.38) | 0.005(1.57 × 10$^{-3}$) |
| 1Y | 39.0(3.09) | 1.40(0.27) | 2.32(0.45) | 0.008(1.95 × 10$^{-3}$) |
| 2Y | 38.6(0.06) | 1.63(0.01) | 2.25(0.66) | 0.007(1.99 × 10$^{-3}$) |
| *CS mortar* | | | | |
| 7D | 36.8(2.18) | 1.61(0.03) | 2.91(0.48) | 0.010(4.40 × 10$^{-3}$) |
| 15D | 37.8(1.58) | 1.63(0.04) | 2.32(0.43) | 0.008(1.66 × 10$^{-3}$) |
| 28D | 32.8(3.34) | 1.65(0.06) | 3.10(1.18) | 0.027(16.3 × 10$^{-3}$) |
| 2M | 34.3(3.39) | 1.65(0.02) | 3.62(0.31) | 0.029(3.00 × 10$^{-3}$) |
| 6M | 37.4(0.25) | 1.62(0.01) | 3.69(0.06) | 0.010(4.16 × 10$^{-3}$) |
| 1Y | 35.7(0.22) | 1.67(0.01) | 2.37(0.23) | 0.008(0.54 × 10$^{-3}$) |
| 2Y | 35.3(0.73) | 1.68(0.01) | 2.13(0.64) | 0.006(3.61 × 10$^{-3}$) |

7D, 7 days; 15D, 15 days; 28D, 28 days; 2M, 2 months; 6M, 6 months; 1Y, 1 year; 2Y, 2 years. Standard deviation of each value is given in parentheses.

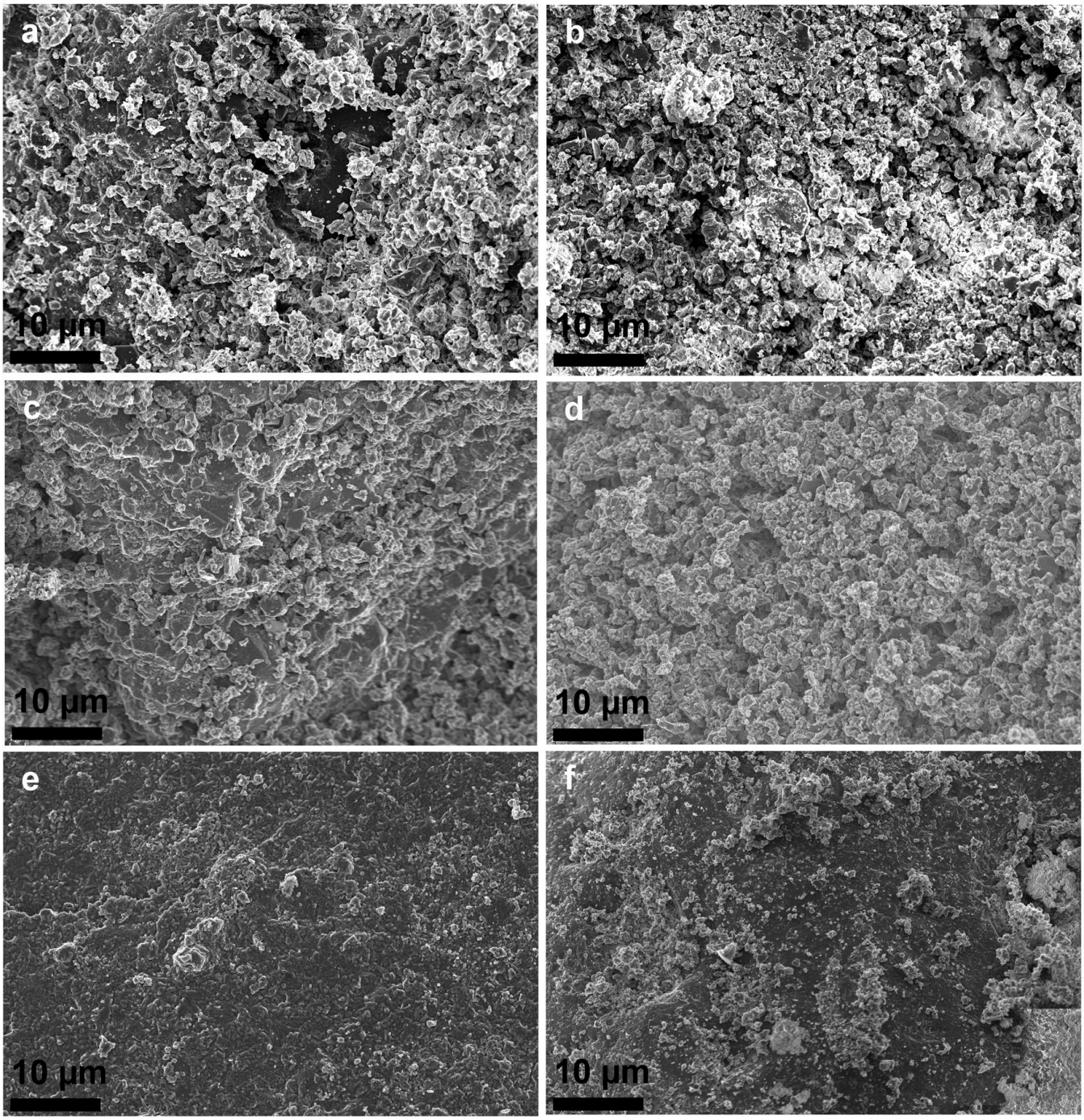


**Fig. 4.** FESEM images of CC (lime mortar with calcareous aggregate) (**a**, **c**, **e**) and CS (lime mortar with siliceous aggregate) (**b**, **d**, **f**) mortars after 28 days (**a**, **b**), 1 year (**c**, **d**) and 2 years (**e**, **f**).

radii (from 0.41 to 0.48 μm) and the volume of pores within this range increased. During the following 5 months, the volume of these pores increased but their size did not. After 1 year, the main peak has the same shape (size and volume) as observed after the first 2 weeks of carbonation. Despite this, the main radius of pores is unchanged with time, hence these variations can be linked to the heterogeneity of the pore network more than to the carbonation process.

The porosity values of CS mortars are fairly constant in the first month of carbonation and only slightly higher after 1 year. CS mortars show a smaller volume of nanopores (Fig. 5c) as well as of pores with radius between 0.1 and 1 μm (Fig. 5d), owing to the fact that less kneading water was used in the preparation of these mortars (see above). Nevertheless, CS mortars are characterized by a much greater volume of larger pores ($1 < r < 10$ μm) than CC mortars, owing to the poor cohesion found at the ITZ of CS samples (see the section on textural characteristics of mortars) caused by both the less continuous grading and the smooth surface of the siliceous aggregate grains. In CC mortars, the presence of large pores at the ITZ was observed only after 7 days of curing, as the PSD curve at this time also confirms (Fig. 5b). PSD curves obtained for CC at other time intervals do not show the presence of large pores and this indicates, once more, that these pores are filled by newly formed calcite.

In both mortars the specific surface area (SSA, Table 3) decreases from 1 year of carbonation onwards and almost no differ-

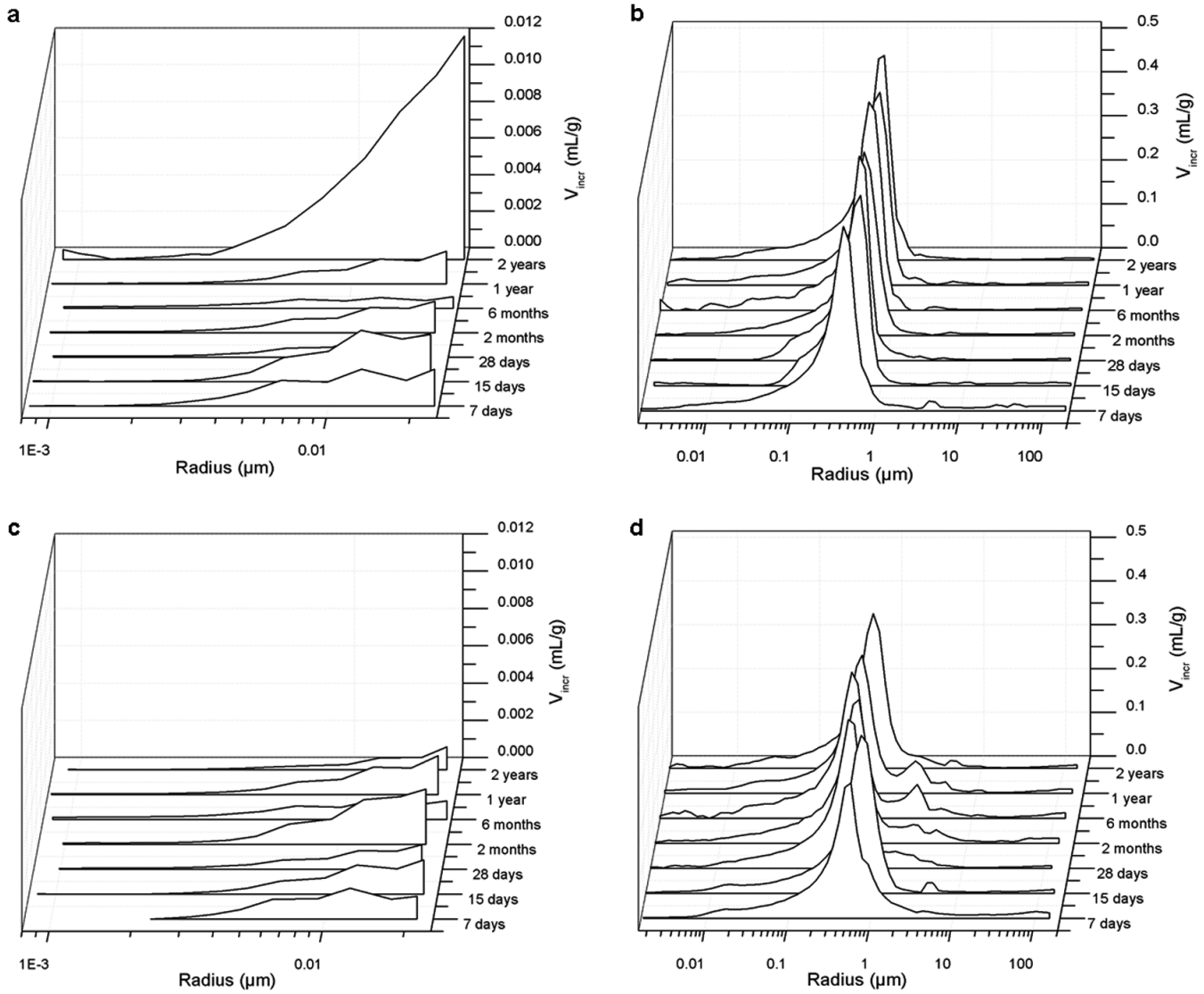


**Fig. 5.** Pore-size distribution curves of CC (lime mortar with calcareous aggregate) and CS (lime mortar with siliceous aggregate) mortars determined after 7, 15 and 28 days, 2 and 6 months, and 1 and 2 years of carbonation. Curves in (**a**) and (**c**) were determined with the BJH method, whereas curves in (**b**) and (**d**) were determined by means of the MIP technique. In all curves, the incremental volume (ml $g^{-1}$) of pores is plotted against their radius (μm).

ences were found in the SSA values of CC and CS. However, the SSA value of the CC mortar is higher in samples after 28 days of curing, as the calcareous aggregate has a higher specific surface area (see the section on water dosage of the mortars). In the same way, the volume of nanopores obtained by $N_2$ adsorption increases until 28 days in CC and 2 months in CS mortars, after which it decreases again.

## Hygric properties

As expected because of the higher porosity of CC mortars, these absorb a higher quantity of water than CS ones when they are immersed in water, but this quantity decreases for both mortars as carbonation progresses (see $C_a$ values, Table 4). In samples with 28 days of curing, CC and CS appear to be saturated after around 10 h of the free water absorption test (insets of Fig. 6a and b). None the less, mortar samples continue absorbing water very slowly over the next 3 days. This second slope of the mass uptake curve, owing to a very slow water absorption, is more pronounced in CC mortars and reflects the differences in the volume of pores between mortars detected by MIP (see the previous section). The presence of small pores causes the decrease in the absorption rate (especially visible in 1-year-old samples) as has already been observed by Martys & Ferraris (1997).

As regards drying, more than one slope is observed in the curves of CC and CS samples, especially in samples with 1 year of carbonation, which dry more slowly than samples that have been cured for shorter periods (Fig. 6a and b), as indicated in the $I_d$ values for mortar samples (Table 4). This results in a worsening of the hygric properties of both mortars, because a slower drying means that water is retained longer in the mortar pore system, thus affecting the durability of the mortars. This occurred especially in CS mortars, where the two slopes are more clearly visible. This behaviour is linked with the pore system of CS samples, which is characterized by a greater volume of large pores ($1 < r < 10$ μm) connected to smaller pores ($0.1 < r < 1$ μm; see the previous section). In this type of network, larger pores are the first to empty, whereas smaller pores remain full of liquid and dry more slowly (Scherer 1990).

Another consideration that must be drawn from these curves regards the absorption and drying ability of mortars during carbonation. A high

**Table 4.** *Absorption coefficient ($C_a$), drying index ($I_d$) and imbibition coefficients (A and B) of CC and CS mortars at different time intervals*

| Time (days) | $C_a$ (g min$^{-1/2}$) | $I_d$ | $A$ (g cm$^{-2}$ min$^{-1/2}$) | $B$ (cm min$^{-1/2}$) |
|---|---|---|---|---|
| *CC mortar* | | | | |
| 28D | 12.67(0.43) | 0.68(0.01) | 0.03(0.00) | 3.25(0.22) |
| 2M | – | – | 0.07(0.00) | 9.72(0.11) |
| 6M | 8.03(0.11) | 0.88(0.00) | 0.08(0.00) | 7.47(1.55) |
| 1Y | 11.92(0.52) | 0.80(0.03) | 0.09(0.00) | 8.33(1.14) |
| 2Y | – | – | 0.07(0.01) | 8.77(0.30) |
| *CS mortar* | | | | |
| 28D | 11.00(0.53) | 0.77(0.01) | 0.06(0.00) | 8.45(0.19) |
| 2M | – | – | 0.06(0.01) | 8.89(0.09) |
| 6M | 7.29(0.19) | 0.88(0.01) | 0.07(0.01) | 7.20(1.23) |
| 1Y | 11.09(0.06) | 0.80(0.02) | 0.07(0.00) | 9.63(0.10) |
| 2Y | – | – | 0.05(0.00) | 7.43(0.03) |

–, Absorption and desorption tests were not performed at 2 months and 2 years of carbonation. Standard deviation of each value is given in parentheses.

absorption of water is obtained in samples carbonated for 28 days, as a consequence of the higher porosity and shrinkage fissures of samples at this age, as was also found by Martys & Ferraris (1997) in mortars and concrete. The decrease in the amount of water absorbed in samples with 6 months of curing seems in contrast to the increase in open porosity observed by MIP from 2 to 6 months of carbonation (Table 3). However, if one observes the PSD curves for both mortars (Fig. 5b and d) it can be seen that in this period the volume of pores with a radius of between 0.01 and 0.15 μm decreased, which indicates that these pores do influence water absorption in mortars. Finally, after 1 year of carbonation, water absorption was similar to that obtained at 28 days in both mortars.

Also, the amount of water absorbed by capillary action (imbibition) is higher in CC mortars than in CS mortars (Fig. 6c and d). This process is slow in CC samples with 28 days of carbonation, as indicated by the lowest $A$ value (Table 4). A partial dissolution of portlandite in water occurred in fresh samples and this slowed down the water rise. In mortar samples after 2 months, 6 months and 1 year, water capillary uptake is faster than in less cured samples (28 days) (Fig. 6c). Despite this, the capillary uptake in 2-year-old samples slows down again, especially in CS samples (Fig. 6d). These observations are confirmed by the values of the $A$ imbibition coefficient presented in Table 4.

The capillary front reaches the top of the samples after 6 h in CC and after 8 h in CS, as shown in Figure 6e and f. None the less, this visual saturation does not coincide exactly with real saturation, which occurs 3 h later as the mass uptake curves show (Fig. 6c and d). This small time-lag between visual and real saturation of the sample indicates that although the water has already reached the top of the sample (as shown in Fig. 6e and f), it continues filling the pores at a slower rate because of the presence of different pore ranges. When all connected pores are filled the sample stops absorbing water and mass saturation is achieved. However, the pore network of both types of mortar can be considered fairly homogeneous (the majority of pores are between 0.1 and 1 μm; see the previous section) because the capillary ascent and mass uptake represented as a function of the square root of time are linear in the majority of the samples (Beck *et al.* 2003) and the time-lag between visual and real saturation is not as large as in other heterogeneous materials (such as tuff) that are characterized by a higher volume of large pores.

It is important to bear in mind that the interpretation of hygric tests in mortars is often complicated by the fact that portlandite can dissolve during water absorption, especially during the first months of mortar life. Clear evidence of this can be seen in Figure 7, in which part of a 28-day-old mortar sample dissolved when water was forced into it. Interestingly, the non-dissolved zone is located at the border of the sample and is 4 mm deep. This indicates the advancing carbonation margin (from the surface to the core; Cazalla 2002; Lawrence *et al.* 2006). In the same way, during capillary processes in the CS samples, two zones were clearly distinguished on the top surface, one saturated and the other still dry. The wet zone formed a contour at the edges of the surface, which resembled the carbonation border. In CC samples, saturation was reached in a more uniform way and no clear border was perceived. The presence of carbonated and non-carbonated zones in mortars produces a heterogeneity that directly affects the hygric properties of the mortars.

## Mechanical properties

As has been observed in other studies (Lanas & Alvarez-Galindo 2003; Arizzi *et al.* 2011), mortars prepared with calcareous aggregate (CC) show higher density and mechanical strengths compared with those prepared with siliceous aggregate (CS) (Fig. 8a). The cause of better cohesion of CC mortars is dependent upon two main factors: the more continuous grading of CA aggregate, which induces better cohesion between aggregate grains and matrix, and the good compositional continuity that exists at the interface between the calcite crystals of the aggregate and the newly formed calcite crystals of the matrix (Cultrone *et al.* 2007). This crystallographic continuity does not exist in CS mortars, which are indeed more fragile and show a high tendency to pulverize during and after rupture, especially when these are submitted to mechanical tests when only 1 month old.

Mortar strength increases during the carbonation process, especially during the first 6 months, after which resistance values remain fairly constant.

The way in which mortars broke during compressive tests is shown schematically in Figure 8b. In mortars, the first visible effect of the compressive strength applied along the direction perpendicular to the compaction plane is the detachment of superficial layers. It is well known that the carbonation process causes mortars to develop high mechanical resistance (owing to the increase in density and the decrease in porosity). Nevertheless, this higher strength does not develop at the same time throughout the whole material but shows better development in the outer carbonated part (Arizzi *et al.* 2011). A lower degree of cohesion exists between the carbonated and the non-carbonated zone of the sample, as demonstrated by the fact that fractures mostly develop at this interface. This heterogeneity causes the type of rupture shown in Figure 8b (outer layers break off) and it is not expected to decrease over time because, as the same authors have observed in similar mortars (Arizzi *et al.* 2011), the differences of Young's modulus between the internal and external samples increase with carbonation.

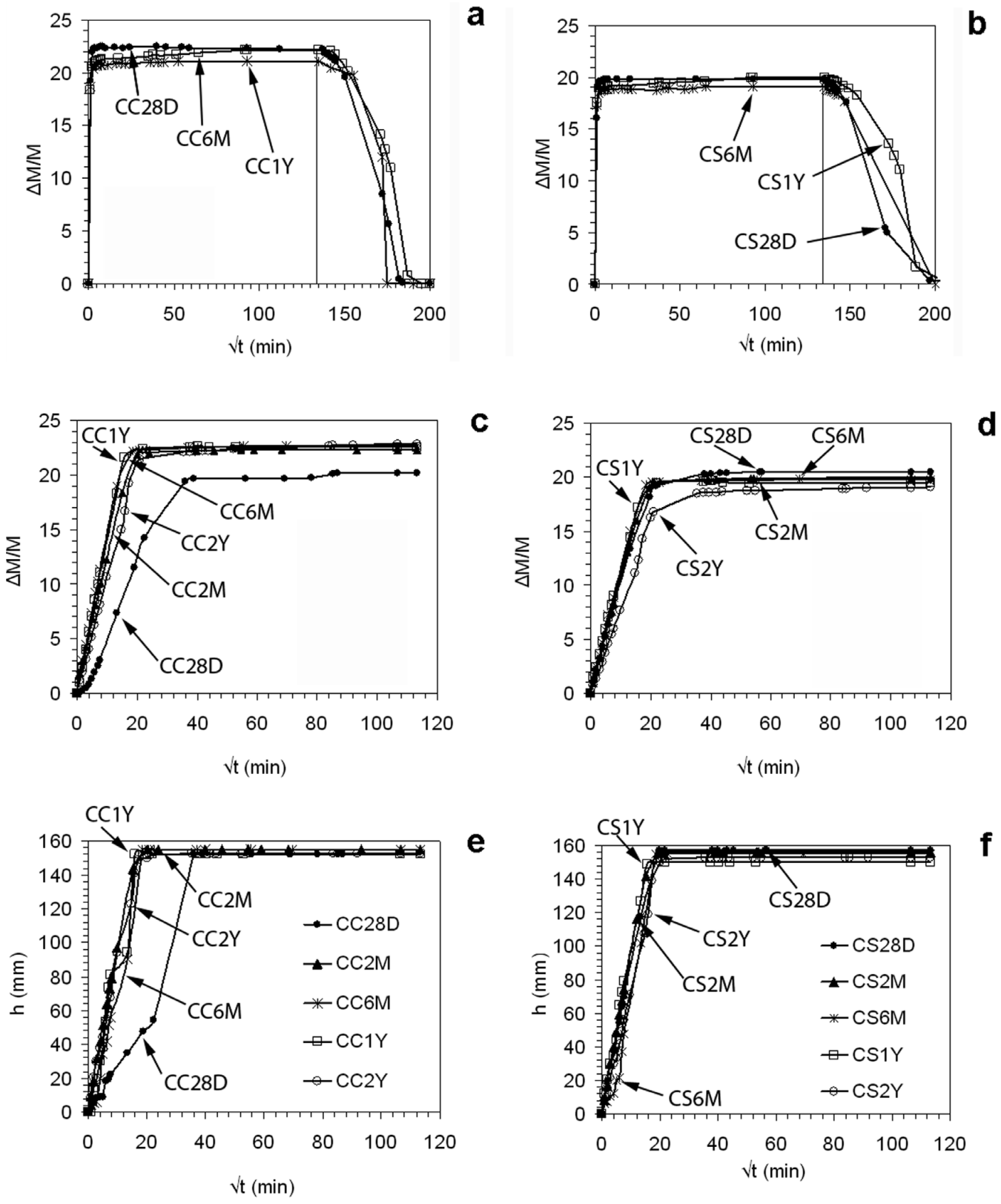


**Fig. 6.** Free water absorption and drying curves of CC (lime mortar with calcareous aggregate) (**a**) and CS (lime mortar with siliceous aggregate) (**b**) mortars after 28 days (-28D), 6 months (-6M) and 1 year (-1Y) of carbonation; time ($\sqrt{t}$, in $min^{-1/2}$) is plotted versus the weight increase ($\Delta M/M$, in %); the vertical line in (**a**) and (**b**) indicates the beginning of the free water drying of mortar samples; Capillarity curves of CC (lime mortar with calcareous aggregate) (**c**, **e**) and CS (lime mortar with siliceous aggregate) (**d**, **f**) mortars after 28 days (-28D), 2 months (-2M), 6 months (-6M), 1 year (-1Y) and 2 years (-2Y) of carbonation; time ($\sqrt{t}$, in $min^{-1/2}$) is plotted versus the weight increase ($\Delta M/M$, in %) (**c**, **d**) and the water uptake level ($h$, in mm) (**e**, **f**).

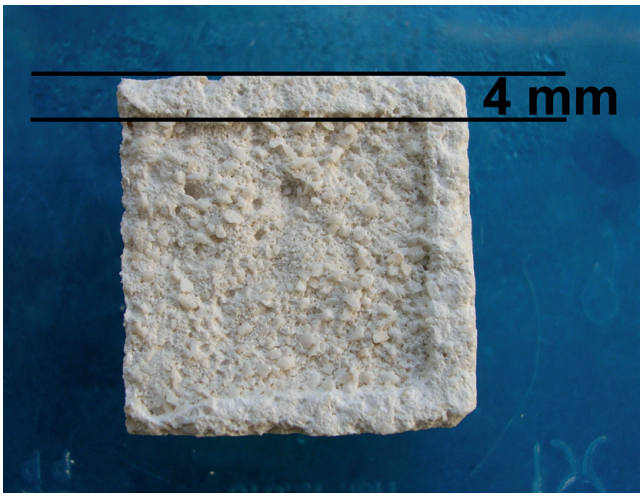


**Fig. 7.** Appearance of the mortar samples when water is forced into the mortar. The dissolved part marks a clear edge of about 4 mm that highlights a carbonation border.

Ultrasound propagates more rapidly in CC mortars and the increase in velocity is higher in these mortars than in CS, especially after 6 months (Fig. 8c and d). Arizzi *et al.* (2013) found a close correspondence between the P-wave propagation velocity ($V_p$) and the carbonation degree of mortars, whereas no direct relation was found between $V_p$ and the aggregate grading and mineralogy. This similarity is clear if one compares the curves in Figures 3 and 8c, in which a common initial steep slope can be seen during the first month, followed by a slight and almost constant slope until 2 years of carbonation. This common trend confirms that the carbonation process induces microstructural changes that have a direct effect on the macroscopic properties of mortars (Arizzi *et al.* 2013). In addition, the most carbonated mortars at the end of the study are also the strongest and the most compact, which is the case of CC mortars. This tight correlation with the degree of carbonation of the mortars was not found for the $V_s$ values, although this parameter also increases over time (Fig. 8d). However, the study of $V_s$ value has been dismissed by other researchers (Benavente *et al.* 2006; Martínez-Martínez 2008) because secondary waves (S) proved to be useless for the characterization of stone materials.

As shown in Table 5, the elastic moduli values for the mortars increase over time and this coincides with the improvement in the cohesion and density of mortars. In general, CS mortars are characterized by slightly higher elastic moduli values, although this is more probably due to the different composition of the aggregate than to the microstructure of the mortars. The exception in this general trend is the Poisson ratio value, which decreases after 1 year of carbonation. These variations are probably due to the variability of the bulk density values (Table 3) used for calculating these moduli, which demonstrate the high heterogeneity of mortar samples. The high variability of the dynamic–mechanical values here reported is reflected in the standard deviation of the $V_p$ values (represented as error bars in Fig. 8c).

## Conclusions

In this study the influence of the aggregate characteristics in the carbonation process of aerial lime mortars has been investigated in detail. A dry hydrated lime and two aggregate types (calcareous and siliceous) were used to prepare mortar samples. The study of the mineralogical and textural characteristics of the aggregates and their relationship with the carbonation of lime helped us to understand the differences in the physical–mechanical properties of mortars and their evolution over time. The main findings on the relationship between the aggregate characteristics and the mortar properties are as follows.

(1) The carbonation degree index, which combines and contrasts the results provided by X-ray diffraction and thermogravimetric analyses, has been shown to be an accurate method for studying the evolution of the carbonation process on the surface and in the core of mortars. Results showed that the transformation of portlandite into calcite occurs mainly in the first 2 months after preparation of the mortars, after which the transformation rate falls sharply. Mortars made with a well-graded calcareous aggregate with rough and angular grains are more carbonated than those made with a less well-graded siliceous aggregate with polished and rounded grains, both on the outer part and in the core of the samples. This is due to two main factors: the better packing and cohesion achieved with the first type of aggregate; and the active role of a calcareous aggregate in the transformation of portlandite into calcite because of a compositional similarity and the presence of cavities on the grain surface, which act as nucleation sites for the new-formed calcite. After 2 years, 3–6% of non-carbonated binder was found in all the samples, confirming how slow the carbonation process is in aerial lime mortars.

(2) The specific surface area values indicate that the water required during the preparation of the mortars also varies depending on the aggregate used; for the same reasons as discussed in the previous point, the calcareous aggregate requires more water than the siliceous one. This leads to the formation of a larger amount of pores (a higher porosity) in the mortars made with calcareous aggregate, owing, above all, to the shrinkage fissures observed in these mortars at the beginning of their life. However, in mortars with calcareous aggregate, the cohesion at the interface between the binder and the aggregate is greatly improved during carbonation and this is reflected in the pore-size distribution of mortars at the following time intervals. Three families of pores have been observed: the main family contains pores of between 0.1 and 1 μm and its volume is greater in mortars made with calcareous aggregate because they require more water; a second group of pores with a radius of more than 1 μm is obtained in mortars made with calcareous aggregate only after 7 days, whereas it is present in mortars made with siliceous aggregate throughout the study; a third peak of smaller pores (ranging between 0.01 and 0.15 μm) is produced as a result of the formation of calcite and its height increases especially in the first months, when carbonation is faster. This phenomenon is particularly evident in mortars made with calcareous aggregate because of the growth of new micrometre-sized calcite crystals on the surface of the calcite grains.

(3) The heterogeneous pore network of mortars is also reflected in the hygric properties of mortars. The higher absorption observed in mortars made with calcareous aggregate suggests that pores with a radius of between 0.1 and 1 μm have the greatest influence on capillary uptake, as this type of mortar has a larger volume of these pores. Furthermore, the volume of pores with a radius of between 0.01 and 0.15 μm influences the amount of water absorbed during the free water absorption test. Pores larger than 1 μm have less influence on total water uptake but they play an important role in the capillary absorption rate. In this sense, mortars with siliceous aggregate absorb water more slowly than those with calcareous aggregate, as the former have a larger volume of large pores. Finally, we found that the heterogeneity of mortar samples is increased by the partial dissolution of portlandite in water during hygric tests, especially in fresh samples (i.e. low-carbonated samples), and this further affects the water absorption kinetics in mortars.

(4) The greater density of mortars made with calcareous aggregate, produced by a faster carbonation process in these samples, induces higher mechanical resistance and propagation velocity of ultrasound within the material. A close relationship has been found between the carbonation degree index of mortars with calcareous and siliceous aggregates and the evolution of the propagation velocity within these mortars over time.

This research not only demonstrates that the aggregate characteristics (mineralogy, morphology, grading and shape) influence the evolution of mortar properties (carbonation, porosity, hygric behaviour, mechanical resistance) but it also shows the way in which this happens. This is crucial for selection of the most suitable aggregate

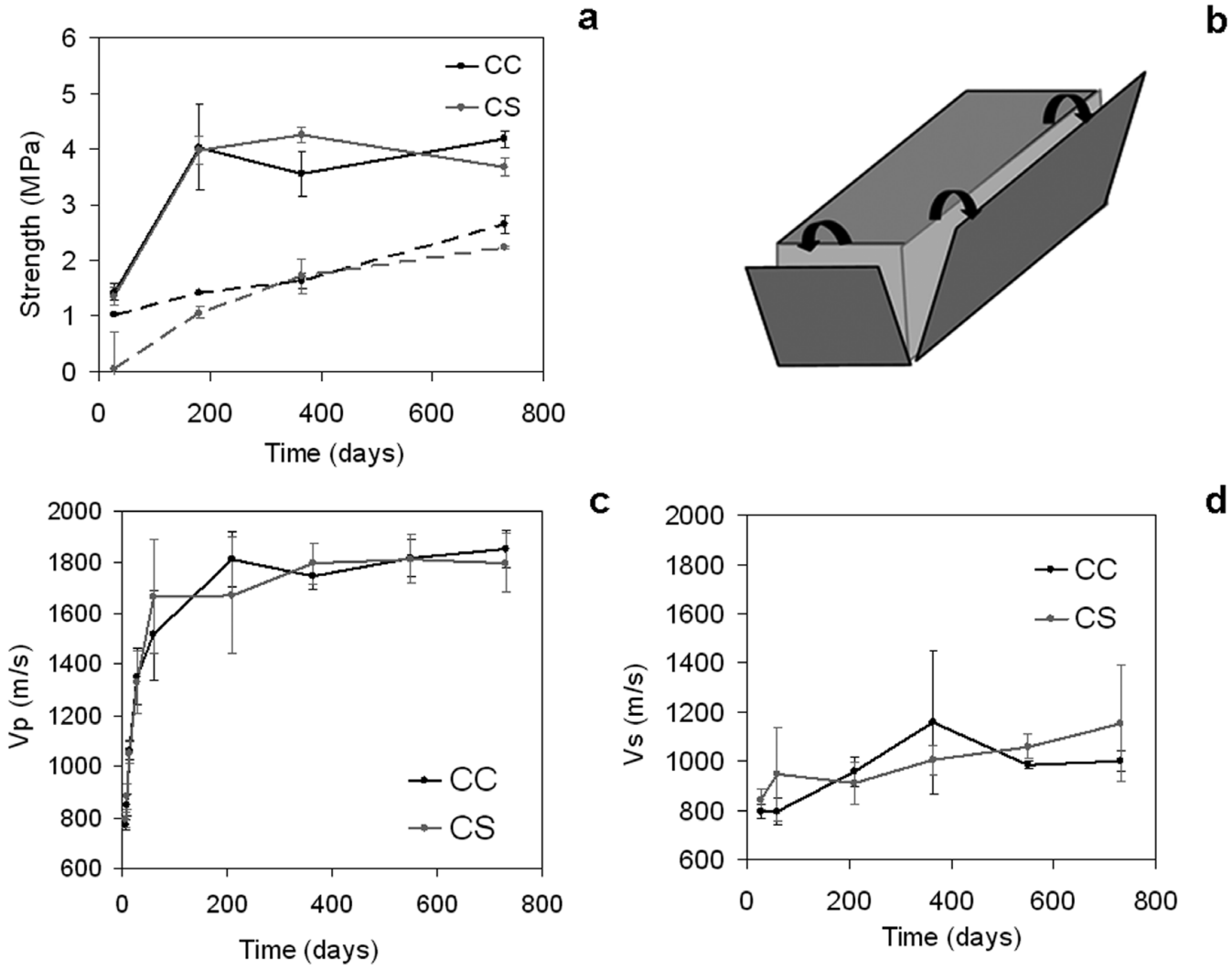


**Fig. 8.** (**a**) Mechanical strengths (in MPa) of CC (lime mortar with calcareous aggregate) and CS (lime mortar with siliceous aggregate) mortars. Continuous and dotted lines refer to compressive and tensile strength, respectively. (**b**) Rupture in sheets of a mortar sample after the compressive test. (**c**, **d**) Velocity of P waves ($V_p$, in $m s^{-1}$) (**c**) and S waves ($V_s$, in $m s^{-1}$) (**d**) in CC (lime mortar with calcareous aggregate) and CS (lime mortar with siliceous aggregate) mortars. Error bars represent the standard deviation of the values at each time interval.

**Table 5.** *Poisson ratio (ν), rigidity modulus (*G*), Young's modulus (*E*) and volume (or compressive) modulus (K) of CC and CS mortars at different time intervals*

| Time (days) | ν | *G* (MPa) | *E* (MPa) | *K* (MPa) |
|---|---|---|---|---|
| *CC mortar* | | | | |
| 28D | 0.23 | 1.01 | 2.49 | 1.56 |
| 2M | 0.31 | 1.04 | 2.72 | 2.39 |
| 6M | 0.31 | 1.38 | 3.60 | 3.11 |
| 1Y | 0.11 | 1.88 | 4.16 | 1.78 |
| 2Y | 0.29 | 1.64 | 4.23 | 3.42 |
| *CS mortar* | | | | |
| 28D | 0.16 | 1.17 | 2.73 | 1.35 |
| 2M | 0.26 | 1.47 | 3.72 | 2.59 |
| 6M | 0.29 | 1.34 | 3.45 | 2.73 |
| 1Y | 0.27 | 1.61 | 4.10 | 3.01 |
| 2Y | 0.15 | 2.23 | 5.14 | 2.46 |

to design a mortar with specific requirements. As a general conclusion for aerial lime-based mortars the selection of an aggregate with a continuous grading, angular shape and surface texture are of high importance with regard to promotion of carbonation and induction of good physical–mechanical properties. This study suggests that where a local supply of a calcareous aggregate can meet these requirements, the use of this aggregate may be more appropriate than a siliceous aggregate that does not. Furthermore, the study also indicates that compositional continuity between calcite aggregate and calcite mortar further improves mechanical properties and the

rate of carbonation. However, further studies comparing aggregates of different mineralogy but comparable gradings would be required to fully support the latter conclusion.

**Acknowledgements.** This study was funded by the Research Group RNM179 of the Junta de Andalucía and by Research Project P09-RNM-4905. We are grateful to Argos Derivados del Cemento, S.L. for providing the raw materials used in this study. We also thank P. Beetham of Loughborough University for the useful comments and suggestions made throughout the revision process of this paper.

## References

AENOR, 1996. *UNE EN 933–2: Tests for Geometrical Properties of Aggregates—Part 2: Determination of Particle Size Distribution—Test Sieves, Nominal Size of Apertures*. AENOR, Madrid.

AENOR, 1997. *UNE EN ISO 11358: Thermogravimetry (TG) of Polymers—General Principles*. AENOR, Madrid.

AENOR, 1999*a*. *UNE EN 1015-2: Methods of Test for Mortar for Masonry—Part 2: Bulk Sampling of Mortars and Preparation of Test Mortars*. AENOR, Madrid.

AENOR, 1999*b*. *UNE EN 1015-3: Methods of Test for Mortar for Masonry. Determination of Consistence of Fresh Mortar (by flow table)*. AENOR, Madrid.

AENOR, 2000. *UNE EN 1015-11: Methods of Test for Mortar for Masonry. Part 11: Determination of Flexural and Compressive Strength of Hardened Mortar*. AENOR, Madrid.

AENOR, 2002. *UNE EN 459-1: Description Building Lime—Part 1: Definitions, Specifications and Conformity Criteria*. AENOR, Madrid.

Arandigoyen, M., Pérez Bernal, J.L., Bello López, M.A. & Alvarez, J.I. 2005. Lime-pastes with different kneading water: Pore structure and capillary porosity. *Applied Surface Science*, **252**, 1449–1459.

Arandigoyen, M., Bicer-Sismir, B., Alvarez, J.I. & Lange, D.A. 2006. Variation of microstructure with carbonation in lime and blended pastes. *Applied Surface Science*, **252**, 7562–7571.

Arizzi, A., Martínez-Martínez, J., Cultrone, G. & Benavente, D. 2011. Mechanical evolution of lime mortars during the carbonation process. *Key Engineering Materials*, **465**, 483–487.

Arizzi, A., Viles, H. & Cultrone, G. 2012. Experimental testing of the durability of lime-based mortars used for rendering historic buildings. *Construction and Building Materials*, **28**, 807–818.

Arizzi, A., Martínez-Martínez, J. & Cultrone, G. 2013. Ultrasonic wave propagation through lime mortars: An alternative and non-destructive tool for textural characterization. *Materials and Structures*, **46**, 1321–1335.

Azconegui, F., Garcia, O. & Martin, M. 1998. *Guía práctica de la cal y el estuco*. Editorial de los Oficios, Leon.

Barret, E.P., Joyner, L.-J. & Halenda, P. 1951. The determination of pore volume and area distributions in porous substances. I. Computations from nitrogen isotherms. *Journal of the American Chemical Society*, **73**, 373–380.

Beck, K., Al-Mukhatar, M., Rozenbaum, O. & Rautureau, M. 2003. Characterization, water transfer properties and deterioration in tuffeau: Building material in the Loire valley, France. *Buildings and Environment*, **38**, 1151–1162.

Benavente, D., Martínez-Martínez, J., Jáuregui, P., Rodríguez, M.A. & García Del Cura, M.A. 2006. Assessment of the strength of building rocks using signal processing procedures. *Construction and Building Materials*, **20**, 562–568.

Bourdette, B., Ringot, E. & Ollivier, J.P. 1995. Modelling of the transition zone porosity. *Cement and Concrete Research*, **25**, 741–751.

Brunauer, S., Emmett, P.H. & Teller, J. 1938. Adsorption of gases in multimolecular layers. *Journal of the American Chemical Society*, **60**, 309–319.

Cazalla, O., Rodriguez-Navarro, C., Sebastian, E. & Cultrone, G. 2000 Aging of lime putty: effects on traditional lime mortar carbonation. *Journal of the American Ceramics Society*, **83**, 1070–1076.

Cazalla, O. 2002. *Morteros de cal. Aplicación en el Patrimonio Histórico*. PhD thesis, University of Granada.

Cizer, O., Rodriguez-Navarro, C., Ruiz-Agudo, C., Elsen, J., Van Gemert, D. & Van Balen, K. 2012. Phase and morphology evolution of calcium carbonate precipitated by carbonation of hydrated lime. *Journal of Materials Science*, **47**, 6151–6165.

CNR-ICR. 1988. *Normal 29-88. Measurement of the Drying Index*. CNR-ICR, Rome.

CNR-ICR, 2008. *UNI EN 13755. Natural Stone Test Methods—Determination of Water Absorption at Atmospheric Pressure*. CNR-ICR, Rome.

Cultrone, G., Sebastian, E. & Ortega Huertas, M. 2007. Durability of masonry systems: A laboratory study. *Construction and Building Materials*, **21**, 40–51.

El-Turki, A., Ball, R.J., Holmes, S., Allen, W.J. & Allen, G.C. 2010. Environmental cycling and laboratory testing to evaluate the significance of moisture control for lime mortars. *Construction and Building Materials*, **24**, 1392–1397.

Fung, W.W.S., Kwan, A.K.H. & Wong, H.H.C. 2008. Wet packing of crushed rock fine aggregate. *Materials and Structures*, **42**, 631–643.

Gomez-Villalba, L.S., Lopez-Arce, P. & Fort, R. 2012. Nucleation of $CaCO_3$ polymorphs from a colloidad alcoholic solution of $Ca(OH)_2$ nanocrystals exposed to low humidity conditions. *Applied Physics A, Materials Science and Processing*, **106**, 213–217.

Gonçalves, J.P., Tavares, L.M., Toledo Filho, R.D., Fairbairn, E.M.R. & Cunha, E.R. 2007. Comparison of natural and manufactured fine aggregates in cement mortars. *Cement and Concrete Research*, **37**, 924–932.

Groot, C.J.W.P. 2010. Performance and repair requirements for renders and plasters. *In*: Valek, J., Groot, C. & Hughes, J. (eds) *International Workshop on 'Repair Mortars for Historic Masonry', RILEM TC 203-RHM, Prague*. RILEM Publications SARL, Bagneux, France, 1359–1363.

Houst, Y.F. & Wittmann, F.H. 1994. Influence of porosity and water content on the diffusivity of $CO_2$ and $O_2$ through hydrated cement paste. *Cement and Concrete Research*, **24**, 1165–1176.

Kwan, A.K.H. & Fung, W.W.S. 2009. Packing density measurement and modelling of fine aggregate and mortar. *Cement and Concrete Composites*, **31**, 349–357.

Lanas, J. & Alvarez-Galindo, J. 2003. Masonry repair lime-based mortars: Factors affecting the mechanical behaviour. *Cement and Concrete Research*, **33**, 1867–1876.

Lawrence, R.M.H., Mays, T.J., Walker, P. & D'Ayala, D. 2006. Determination of carbonation profiles in non-hydraulic lime mortars using thermogravimetric analysis. *Thermochimica Acta*, **444**, 179–189.

Lawrence, R.M., Mays, T.J., Rigby, S., Walker, P. & D'Ayala, D. 2007. Effects of carbonation on the pore structure of non-hydraulic lime mortars. *Cement and Concrete Research*, **37**, 1059–1069.

Martín Ramos, J.D. 2004. XPowder. A software package for powder X-ray diffraction analysis. Lgl. Dep. GR 1001/04, University of Granada, Spain.

Martínez-Martínez, J. 2008. *Influencia de la alteración sobre las propiedades mecánicas de calizas, dolomías y mármoles. Evaluación mediante estimadores no destructivos (ultrasonidos)*. PhD thesis, University of Alicante.

Martys, N.S. & Ferraris, C. 1997. Capillary transport in mortars and concrete. *Cement and Concrete Research*, **27**, 747–760.

Moorehead, D.R. 1986. Cementation by the carbonation of hydrated lime. *Cement and Concrete Research*, **16**, 700–708.

NHBC Foundation 2008. *The Use of Lime-Based Mortars in New Build*. IHS BRE Press, Watford.

Ngala, V.T. & Page, C.L. 1997. Effects of carbonation on pore structure and diffusional properties of hydrated cement pastes. *Cement and Concrete Research*, **27**, 995–1007.

Rodriguez-Navarro, C. & Doehne, E. 1999. Salt weathering: Influence of evaporation rate, supersaturation and crystallization pattern. *Earth Surface Processes Landforms*, **24**, 191–209.

Rodriguez-Navarro, C., Cazalla, O., Elert, K. & Sebastian, E. 2002. Liesegang pattern development in carbonating traditional lime mortars. *Proceedings of the Royal Society of London*, **458**, 2261–2273.

Rodriguez-Navarro, C., Ruiz Agudo, E., Ortega Huertas, M. & Hansen, E. 2005. Nanostructure and irreversible colloidal behaviour of $Ca(OH)_2$: Implications in cultural heritage conservation. *Langmuir*, **21**, 10948–10957.

Romagnoli, M. & Rivasi, M.R. 2007. Optimal size distribution to obtain the densest packing: A different approach. *Journal of the European Ceramics Society*, **27**, 1883–1887.

Ruiz Agudo, E. & Rodriguez-Navarro, C. 2010. Microstructure and rheology of lime putty. *Langmuir*, **26**, 3868–3877.

Sánchez-Moral, S., García-Guinea, J., Luque, L., Gonzalez-Martín, R. & López-Arce, P. 2004. Carbonation kinetics in roman-like lime mortars. *Materiales de Construcción*, **275**, 23–37.

Scherer, G.W. 1990. Theory of drying. *Journal of the American Ceramics Society*, **73**, 3–14.

Van Balen, K. 2005. Carbonation reaction of lime, kinetics at ambient temperature. *Cement and Concrete Research*, **35**, 647–657.

Veiga, M.R. 2010. Conservation of historic renders and plasters: from lab to site. *In*: Valek, J., Groot, C. & Hughes, J. (eds) *Proceedings of the 2nd Historic Mortars Conference, Prague*, RILEM Publications SARL, Bagneux, France, 1241–1256.

Venkatarama, B.V.R. & Gupta, A. 2007. Influence of sand grading on the characteristics of mortars and soil–cement block masonry. *Construction and Building Materials*, **22**, 1614–1623.

Westerholm, M., Lagerblad, B., Silfwerbrand, J. & Forssberg, E. 2008. Influence of fine aggregate characteristics on the rheological properties of mortars. *Cement and Concrete Composites*, **30**, 274–282.

Received 29 February 2012; accepted 6 September 2013.